

Potential high- T_c superconductivity in YCeH_x and LaCeH_x under pressure

Peng Song,¹ Zhufeng Hou,² Kousuke Nakano,^{1,3} Kenta Hongo,⁴ and Ryo Maezono¹

¹*School of Information Science, JAIST, Asahidai 1-1, Nomi, Ishikawa 923-1292, Japan*

²*State Key Laboratory of Structural Chemistry, Fujian Institute of Research on the Structure of Matter, Chinese Academy of Sciences, Fuzhou 350002, China*

³*International School for Advanced Studies (SISSA), Via Bonomea 265, 34136, Trieste, Italy*

⁴*Research Center for Advanced Computing Infrastructure, JAIST, Asahidai 1-1, Nomi, Ishikawa 923-1292, Japan*

(Dated: November 15, 2022)

Lanthanum, yttrium, and cerium hydrides are the three most well-known superconducting binary hydrides (La-H, Y-H, and Ce-H systems), which have gained great attention in both theoretical and experimental studies. Recent studies have shown that ternary hydrides composed of lanthanum and yttrium can achieve high superconductivity around 253 K. In this study we employ the evolutionary-algorithm-based crystal structure prediction (CSP) method and first-principles calculations to investigate the stability and superconductivity of ternary hydrides composed of (Y, Ce) and (La, Ce) under high pressure. Our calculations show that there are multiple stable phases in Y-Ce-H and La-Ce-H systems, among which $P4/mmm$ - YCeH_8 , $P\bar{6}m2$ - YCeH_{18} , $R\bar{3}m$ - YCeH_{20} , $P4/mmm$ - LaCeH_8 , and $R\bar{3}m$ - LaCeH_{20} possessing H_{18} , H_{29} and H_{32} clathrate structures can maintain both the thermodynamic and lattice-dynamic stabilities. In addition, we also find that these phases also maintain a strong resistance to decomposition at high temperature. Electron-phonon coupling calculations show that only three of these five phases can exhibit high-temperature superconductivity. The superconducting transition temperatures (T_c) of $R\bar{3}m$ - YCeH_{20} , $R\bar{3}m$ - LaCeH_{20} , and $P\bar{6}m2$ - YCeH_{18} are predicted using the Allen-Dynes-modified McMillan formula to be 122 K at 300 GPa, 116 K at 250 GPa, and 173 K at 150 GPa, respectively. Moreover, the pressure to stabilize $P\bar{6}m2$ - YCeH_{18} can be lowered to 150 GPa, suggesting an accessible condition for its high-pressure synthesis.

I. INTRODUCTION

Superconductivity has gotten a remarkable progress and attention owing to its unique phenomenon and wide range of industrial applications. [1–7] On the other hand, the extremely low temperature environment required for the manifestation of these properties severely limits the breadth of their application. Therefore, the pursuit for high(room)-temperature superconductivity has historically been one of the most competitive and sought goals in superconductivity. [8–10] According to the Bardeen-Cooper-Schrieffer (BCS) theory, the superconducting transition temperature (T_c) significantly correlates with the phonon vibration frequency. [11–14] In this sense, metallic hydrogen is considered to be the most ideal candidate for high- T_c superconductivity due to its ultra-high phonon vibration frequency. [15] However, hydrogen metallization, also known as the Wigner-Huntington transition, typically requires extremely high pressures, making it difficult to study its superconductivity-related electrical properties at these pressures. [16–23] Ashcroft proposed the introduction of other elements into hydrogen can provide the necessary pre-compression for the entire system, allowing it to maintain metallicity and superconductivity at lower pressures. [24] Thus, metal hydrides are one of the most ideal candidates for high- T_c superconductivity.

According to Ashcroft, almost all binary hydrides have been theoretically screened out by density functional theory (DFT) calculations, and some predictions have been verified by experiments. [25–41] Compared to binary superconducting hydrides, research on multi-component superconducting hydrides appears to be slightly less. Since multi-component hydrides contain more combinations of elements, however, they

are more promising in the search for high(room)-temperature superconductivity. [41–61] For example, the DFT calculations by Sun *et al.* [49] predicted that magnesium hydride can dissociate the H_2 molecule into atomic H by lithium doping. This doping increases its electron concentration at the Fermi level (E_F), enabling it to reach a T_c value of 473 K at 250 GPa. [49] Furthermore, a recent high-pressure experiment has revealed that a small amount of carbon doping in H_3S can result in room-temperature superconductivity ($T_c = 287.7 \pm 1.2$ K at 267 ± 10 GPa), [62] although the anomaly of AC susceptibility in low temperature for the carbonaceous sulfur hydride has been questioned by Hirsch *et al.* [63, 64] and more strong experimental data are needed to support the claim of the observation of room-temperature superconductivity. Therefore, increasing the density of electronic states at E_F by electrons doping in the binary hydride can affect the T_c value; however this modification also can result in a decrease in T_c in some cases. [65–67]

Furthermore, most of the high- T_c superconducting hydrides reported thus far are concentrated in the Mendeleev table’s “lability belt”, and many of these hydrides have unusual structural properties, such as a cage-like structure surrounded by H. [25] Some ternary superconducting hydrides (e.g., ScYH_6 , ScCaH_8 , CaYH_{12} , and so on) can be easily obtained by substituting one of the metal atoms in the binary parent compound. [50–54] The crystal structure, pressure range of stability, unit cell volume, and other properties of the parent binary superconducting hydrides that correspond to these ternary superconducting hydrides resemble each other. [10, 25] For instance, by combining two types of binary hydrides with comparable structural features, it is possible to produce a more stable ternary hydride with similar structural proper-

ties. To test this hypothesis, we noticed that CeH₉, YH₉, and LaH₁₀, CeH₁₀ have comparable qualities in a variety of properties, and their structural properties have been proven in high-pressure experiments. [32, 33, 38, 39] The related ternary superconducting hydrides, one of which is (La,Y)H₁₀, has been successfully synthesized experimentally, and the T_c observed under high pressure also matched the theoretically predicted T_c quite well. [54] During this work, we are aware that a very recent high-pressure experiment study shows that La-Ce-H may have stable $I4/mmm$ -(La,Ce)H₄ and $Im\bar{3}m$ -(La,Ce)H₆ around 100 GPa. [68]

Therefore, this work will concentrate on the YCeH_x and LaCeH_x systems, which have not yet been well investigated, to explore whether there exist stable compounds under high pressure. By employing the evolutionary algorithm for crystal structure prediction, we have theoretically discovered thermodynamically stable compounds of YCeH₅, YCeH₇, YCeH₈, YCeH₁₈, YCeH₂₀, LaCeH₈, LaCeH₁₈, and LaCeH₂₀ in pressure range of 100-400 GPa. In addition, we have investigated the dynamic stability and superconductivity of these hydrogen-rich ternary hydrides within the harmonic approximation. All of them are dynamically stable with increasing pressure, More importantly, YCeH₁₈ exhibits extremely strong electron-phonon coupling with superconducting transition temperatures of 173 K at 150 GPa.

II. METHOD

The crystal-structure search for YCeH_x and LaCeH_x ($x = 2\sim 10, 12, 14, 16, 18, \text{ and } 20$) at 100, 200, and 300 GPa was performed using the USPEX (Universal Structure Predictor: Evolutionary Xtallography) [69, 70] code. In the USPEX run, 200 structures with 1-2 formula units were randomly built for the initial generation, and then 100 structures for each of the subsequent generations were produced by 40% heredity, 40% random, 10% mutation, and 10% soft mutation. Each structure was optimized through 4 times of relaxation from low to high accuracy levels. The structure relaxation was carried out by the density functional theory calculations within the generalized gradient approximation (GGA) with Perdew-Burke-Ernzerhof (PBE) exchange-correlation functional [71] as implemented in the VASP (Vienna *ab initio* simulation package) [72, 73] code. The electron-ion interaction was treated using projector-augmented-wave (PAW) potentials. [72, 73] The Ce 4f electrons were explicitly considered into the valence electrons. The cutoff energy for plane waves was set to 600 eV and the smallest allowed spacing between the k -points in the irreducible Brillouin zone was set to be 0.2 Å⁻¹. To study the chemical bonding and electronic structures of some selected stable YCeH_x and LaCeH_x, we have carried out the static calculations using the VASP code and then performed the Crystal Orbital Hamilton Population (COHP) and Crystal Orbital Bond Index (COBI) analyses using the Lobster 4.1.0 package [74] together with the pbeVaspFit2015 basis set. The electronic band structures were also checked by taking into account the spin-orbit coupling (SOC) interaction and the correction of the on-site Coulomb interaction of Ce 4f orbitals.

The DFT+ U method of Dudarev *et al.* [75] was employed in the latter case. The Hubbard U parameter for Ce 4f orbitals was determined by the density-functional perturbation theory approach, as implemented in the HP package [76]. The obtained U for Ce 4f orbitals is 4.2 eV, which is very close to the value (i.e., 4.5 eV) adopted by Wang *et al.* [77] for their study on CeH₉. The exchange interaction parameter J for Ce 4f orbitals was taken from Ref. 77 and set to 0.5 eV.

The formation enthalpies of La-Ce-H and Y-Ce-H ternary systems (herein abbreviated to A-Ce-Y with $A = \text{La}$ and Y), relative to the elemental solids Y [78], Ce [79], La [80], and H [81], were calculated at each pressure defined as below:

$$\Delta\mathcal{H} = \frac{1}{x+y+z} \left[\mathcal{H}(A_x\text{Ce}_y\text{H}_z) - x\mathcal{H}(A) - y\mathcal{H}(\text{Ce}) - z\mathcal{H}(\text{H}) \right], \quad (1)$$

where $\mathcal{H}(A_x\text{Ce}_y\text{H}_z)$ is the enthalpy per formula unit (f.u.) of the A-Ce-H compound; $\mathcal{H}(A)$, $\mathcal{H}(\text{Ce})$, and $\mathcal{H}(\text{H})$ are the reference enthalpies of A, Ce, and H single phases, respectively. The thermodynamic stability of the predicted phase was determined by comparing the formation enthalpies with respect to the convex hull energy:

$$E_{\text{above.hull}} = \Delta\mathcal{H} - \Delta\mathcal{H}_f, \quad (2)$$

where $\Delta\mathcal{H}_f$ is a convex hull energy obtained by constraining the minimum value of the total enthalpies of a linear combination of stable phases [82], which can be computed using the ConvexHull module in scipy. [83] $E_{\text{above.hull}}$ is energy above the convex hull. $E_{\text{above.hull}} = 0$ means that the corresponding ternary phase is stable, namely, such a phase would not decompose into any combination of elementary, binary, or other ternary phases. The Gibbs free energies at finite temperatures were calculated within the quasiharmonic approximation using the PHONOPY code. [84] After incorporating the Gibbs free energies, we can drive the stability for the whole system at high temperatures by computing the convex hull.

The phonon dispersion and electron-phonon coupling (EPC) of the stable ternary phases were carried out using the Quantum ESPRESSO (QE) code [85] with the PAW method and the GGA-PBE exchange-correlation functional. In particular, the Ce PAW potential was generated with a valence configuration of 4d¹⁰5s²5p⁶4f^{0.5}5d^{1.5}6s², as provided by the PSLibrary of Dal Corso [86]. The cutoff energy for plane-wave basis sets in the QE calculations was set to 180 Ry. The q -point mesh (and integral k -points mesh) in the first Brillouin-zone for the EPC calculations was set as follows: $5 \times 5 \times 2$ ($20 \times 20 \times 8$) for ACeH₈, $5 \times 5 \times 3$ ($20 \times 20 \times 12$) for ACeH₁₈ and $4 \times 4 \times 4$ ($20 \times 20 \times 20$) for ACeH₂₀ ($A = \text{La}$ and Y). The the Allen-Dynes-modified McMillan formula (AD) and the Eliashberg function derived from the EPC calculation were used to predict the superconducting critical temperature as follows [87, 88]:

$$T_c = \frac{\omega_{\log} f_1 f_2}{1.2} \exp\left(\frac{-1.04(1+\lambda)}{\lambda(1-0.62\mu^*) - \mu^*}\right), \quad (3)$$

with

$$f_1 f_2 = \sqrt[3]{1 + \left[\frac{\lambda}{2.46(1 + 3.8\mu^*)} \right]^2} \times \left[1 - \frac{\lambda^2(1 - \omega_2/\omega_{\log})}{\lambda^2 + 3.312(1 + 6.3\mu^*)^2} \right]. \quad (4)$$

When $f_1 f_2 = 1$, Eq. (3) is restored to the original McMillan formula (McM). The μ^* is the Coulomb pseudopotential, which is defined as below [88]

$$\mu^* = \frac{\mu}{1 + \mu \log(\omega_{el}/\omega_{ph})}, \quad (5)$$

where μ is instantaneous repulsion, the $\log(\omega_{el}/\omega_{ph})$ is a ratio of propagation time. For most metal compounds, the value of μ^* is roughly in the range of 0.1 to 0.16 by incorporating previous experimental and calculated data. The widely accepted value of 0.1 for μ^* was used herein. The electron-phonon coupling constant (λ), logarithmic average phonon frequency (ω_{\log}), and mean square frequency (ω_2) are defined as below

$$\lambda = 2 \int \frac{\alpha^2 F(\omega)}{\omega} d\omega, \quad (6)$$

$$\omega_{\log} = \exp \left[\frac{2}{\lambda} \int \frac{d\omega}{\omega} \alpha^2 F(\omega) \log \omega \right], \quad (7)$$

and

$$\omega_2 = \sqrt{\frac{1}{\lambda} \int \left[\frac{2\alpha^2 F(\omega)}{\omega} \right] \omega^2 d\omega}, \quad (8)$$

respectively.

III. RESULTS AND DISCUSSION

A. Phase stability and crystal structural of YCeH_x and LaCeH_x

Because predicting the ternary phase diagram in its entirety is computationally expensive, and our main target is to determine the stability and superconductivity of the hydrogen-rich phase, this research focuses on stable compounds and crystal structures at 100 GPa, 200 GPa, and 300 GPa along a line chosen by YCeH_x and LaCeH_x ($x = 2-8, 10, 12, 14, 16, 18, \text{ and } 20$) for the fixed composition search. This approach is currently seen to be effective for alkaline earths and rare earth metal ternary hydrides. [35, 50, 58] For the stability analysis of YCeH_x and LaCeH_x, the corresponding Y-H, La-H, and Ce-H binary hydrides have been extensively studied. [32, 34, 39] Theoretical calculations show that there is a hydrogen-rich structure MH₉ ($M = \text{Y, La, and Ce}$) that can be stabilized below 100 GPa in the three binary systems. In addition, YH₁₀ is capable of exhibiting room temperature superconductivity. [26] Therefore, this study mainly used these

stable binary hydrides as well as single elements as a reference for thermodynamic stability assessment.

The constructed convex hulls of YCeH_x and LaCeH_x at 200 GPa are presented in Fig. 1. Their stable and metastable phases are highlighted by the symbols of circles and red diamond in Fig. 1, respectively. The more detailed results for the stabilities of YCeH_x and LaCeH_x at difference pressures are presented in Figs. S1-S6 in the Supplementary Material (SM). YCeH₅, YCeH₇, YCeH₈, LaCeH₈, and LaCeH₁₈ are found to be stabilized at 100 GPa. When the pressure increases up to 200 GPa, YCeH₅, YCeH₇, and LaCeH₁₈ vanish from the ternary convex, while LaCeH₂₀ and YCeH₁₈ appear in the stable phases of convex hull. In the pressure range of 100-300 GPa, YCeH₂₀ fails to achieve stability. But further increasing the pressure above 300 GPa, $R\bar{3}m$ -YCeH₂₀ becomes stable, and its stable pressure interval is very close to that of YH₁₀. [26] In addition, in the pressure interval of 300-400 GPa, LaCeH₈, LaCeH₂₀, and YCeH₂₀ undergo a phase transition to the more stable $Pm\bar{m}n$, $P6_3/mmc$, and $P4/mmm$ phases, respectively. The ranges of the stabilization pressures of these new predicted phases have been summarized in Fig. 2. To further explore the resistance of these phases to decomposition at high temperatures, we calculated the ternary convex hull at a finite temperature at 200 GPa. We note that the stable phase (YCeH₈, YCeH₁₈, LaCeH₈, and LaCeH₂₀) at this point is also stable at high temperatures, and its specific energy values have been placed in the SM. Therefore, the above-mentioned can be synthesized in the same way as (La,Y)H_x [54] by heating LaCe and YCe alloys with NH₃BH₃ at high pressure.

It is interesting to note that most of the above predicted stable phases, except YCeH₅ and YCeH₇, are composed of clathrate structures enclosed by H. For instance, the clathrate structures of stable YCeH₈, LaCeH₈, YCeH₁₈, LaCeH₁₈, and YCeH₂₀ are shown in Fig. 3. Since the hydrogen-rich compounds are more likely to achieve high- T_c superconductivity [10], the hydrogen-less ones such as YCeH₅ and YCeH₇ will be discussed elsewhere. The stable hydrides of YCeH_x and LaCeH_x with clathrate structures can be roughly divided into three groups.

(i) The first one consists of H₁₈ cages, as found in $P4/mmm$ -YCeH₈, $P4/mmm$ -LaCeH₈, and $Pm\bar{m}n$ -LaCeH₈, which are derived from their corresponding parent compounds ($I4/mmm$ -YH₄, $I4/mmm$ -CeH₄, and $I4/mmm$ -LaH₄) [26] with the same cage structure. If half of Ce atoms at the site $2a$ of the $I4/mmm$ -CeH₄ phase are orderly replaced by Y or La atoms, the $P4/mmm$ ternary phase would be formed. [26] The relative enthalpies of these two structures of LaCeH₄ and YCeH₄ are shown in Figs. S1 and S4. We find that the most stable candidate structures prefer the H₁₈ cages. In addition, LaCeH₈ would be transformed into the $Pm\bar{m}n$ phase when the pressure is above 300 GPa. (ii) The second group consists of H₂₉ cages, as found in the $P\bar{6}m2$ -YCeH₁₈ and $Amm2$ -LaCeH₁₈ phases. The $P\bar{6}m2$ -YCeH₁₈ phase can be derived by replacing half of Ce atoms at the site $2d$ of $P6_3/mmc$ -CeH₉ with Y atoms. As for the parent compounds of $P\bar{6}m2$ -YCeH₁₈ and $Amm2$ -LaCeH₁₈, the previous study by Peng *et al.* [26] has shown that only stable $P6_3/mmc$ -YH₉ and $P6_3/mmc$ -

CeH₉ phases exist in the pressure range of 100-400 GPa, however LaH₉ does not. For the *Amm2*-LaCeH₁₈ phase, only its internal energy plays a superior role to hinder its possible decomposition pathway of $1/6 \text{ LaH}_4 + 1/6 \text{ LaH}_{10} + \text{CeH}_9$, and thus it cannot be stabilized at higher pressures. [26, 89] (iii) The third group consists of the H₃₂ cages, as found in YCeH₂₀ and LaCeH₂₀. The $R\bar{3}m$ -YCeH₂₀ and $R\bar{3}m$ -LaCeH₂₀ phases exhibit the same spatial structure with LaYH₂₀, [54] and all of them are the supercell structures of their parent phases $Fm\bar{3}m$ -AH₁₀. More specifically speaking, the equivalent primitive unit cell of $R\bar{3}m$ -YCeH₂₀ can be obtained by replacing half of Ce atoms with Y atoms in the $1 \times 1 \times 2$ extension of the primitive unit cell of $Fm\bar{3}m$ -CeH₁₀. LaCeH₂₀ undergoes a phase transition from $R\bar{3}m$ to $P6_3/mmc$. For YCeH₂₀, it also undergoes a phase transition at 370 GPa and the new high-pressure phase can be derived by replacing half of Ce atoms in the site 4b of the parent phase $Fm\bar{3}m$ -CeH₁₀ with Y atoms. Considering the chemical similarity of elements, one may choose the stable phases of binary hydrides as the starting structures to accelerate the search for multi-component hydrides.

To further check the lattice dynamic stability of the above predicted YCeH_x and LaCeH_x phases, we have employed the Phonopy [84] code to initially calculate their phonon band structures, which are presented in Fig. S7 in the SM. Among them, the *Amm2*-LaCeH₁₈ phases cannot maintain dynamic stability in the pressure range of their thermodynamic stability. To make the $R\bar{3}m$ -LaCeH₂₀ phase dynamically stable, the pressure needs to be above 200 GPa. In addition, the high pressure applied in the current mainstream experimental studies of metal hydrides falls into a range of 100-300 GPa. As for the phases stabilized above 300 GPa, both $R\bar{3}m$ -YCeH₂₀ and $R\bar{3}m$ -LaCeH₂₀ have a certain degree of similarity. Therefore, we pay much attention to the $P4/mmm$ -YCeH₈, $P\bar{6}m2$ -YCeH₁₈, $R\bar{3}m$ -YCeH₂₀, $P4/mmm$ -LaCeH₈, and $R\bar{3}m$ -LaCeH₂₀ phases for their electronic properties and superconductivity.

B. Electronic Properties and Superconductivity

The electronic band structure, the electronic density of states (eDOS), of $P4/mmm$ -YCeH₈, $P\bar{6}m2$ -YCeH₁₈, $R\bar{3}m$ -YCeH₂₀, $P4/mmm$ -LaCeH₈, and $R\bar{3}m$ -LaCeH₂₀ at high pressures are presented in Figs. S8-S10 in the SM, respectively. All these compounds in the pressure range of their thermodynamical stabilities possess the metallic features in their energy band structures. For $P4/mmm$ -YCeH₈ and $P4/mmm$ -LaCeH₈, there are very steep conduction bands along the $Z \rightarrow \Gamma$ direction crossing the Fermi level (E_F), resulting in electron pockets near the Γ point. For $R\bar{3}m$ -YCeH₂₀ and $R\bar{3}m$ -LaCeH₂₀, a band inversion can be found around the Γ point and near the E_F , which is mainly attributed to the H 1s and Ce 4f orbitals, as seen from the atom- and orbital-weighted band structures in Figs. S8 and S9 in the SM, respectively. The eDOS at E_F (N_{E_F}) for $P4/mmm$ -YCeH₈, $P\bar{6}m2$ -YCeH₁₈, $R\bar{3}m$ -YCeH₂₀, $P4/mmm$ -LaCeH₈, and $R\bar{3}m$ -LaCeH₂₀ are 1.72, 1.39, 1.10, 1.34, and 1.26 states/eV/f.u., respectively. As further analyzed by the atom-projected eDOS, the difference in the aforemen-

tioned values of N_{E_F} mainly comes from the different contribution of H and Ce atoms to the N_{E_F} . The contribution of Ce atoms at E_F is continuously suppressed as the hydrogen content increases, while the opposite trend is observed for H. However, the decrease of Ce is higher than the increase of H, leading to a constant decrease of the total DOS with increasing H content. According to the arguments of Belli *et al.*, [90] the superconductivity of hydrides maintains a strong positive correlation with the contribution of H in the total DOS at E_F (H_{DOS}). The H_{DOS} for these five phases are 9.5%, 34.4%, 38.2%, 11.2%, and 34.7%, respectively. This indicates that the H-rich phase has a higher H-derived DOS at E_F although the corresponding total DOS is low, which may suggest that the possibility of high- T_c in H-rich phases to some extent. [90]

From the orbital-weighted electronic band structures of $P\bar{6}m2$ -YCeH₁₈, $R\bar{3}m$ -YCeH₂₀ and, $R\bar{3}m$ -LaCeH₂₀, as shown in Fig. S9, it can be seen that the bands around E_F are mainly contributed by the hybridization between the Ce 4f and H 1s orbitals. We should point out that they were predicted by the GGA-PBE functional. This raises a question how strong the SOC interaction and the correlated effect would be associated with the Ce 4f orbitals in these compounds. So, we further checked the electronic band structures with the SOC interaction, the correction of the on-site Coulomb interaction of Ce 4f orbitals, and their combination, which are presented in Fig. S10 in the SM. We find that both the SOC interaction and the correction of the on-site Coulomb interaction have much weak effect on the bands around E_F , which could be neglected. The superconducting transition temperature is largely affected by the electronic properties at the E_F . Therefore, the computational methodology employed in the present study would be acceptable to give a reasonable prediction on the superconducting properties of Ce-containing ternary hydrides. The similar treatment with ignoring the SOC interaction and the correlated effect has also been employed in several of the previous theoretical studies [26, 77, 91] on the electron-phonon coupling of binary CeH_x. Unfortunately, the combination of the DFT+ U method and the density-functional perturbation theory approach in the latest version (v7.1) of QE code does not support the electron-phonon interaction calculations. Because of the above reasons, our superconductivity calculations did not consider the SOC interaction and the strongly-correlated effect.

The phonon dispersions with the mode-resolved electron-phonon coupling (EPC) constant λ_{qv} , atom-projected phonon density of states (PHDOS), and EPC spectra of $P4/mmm$ -YCeH₈, $P\bar{6}m2$ -YCeH₁₈, $R\bar{3}m$ -YCeH₂₀, $P4/mmm$ -LaCeH₈, and $R\bar{3}m$ -LaCeH₂₀ at high pressures are presented Fig. 4 and Fig. S12 in the SM. For these five phases, the phonons with frequencies above 10 THz are dominated by the H contribution, accounting for more than 70%. The phonons with frequencies below 10 THz are mainly contributed by La, Ce, and Y atoms. Because of the difference in the atomic masses of Y, La, and Ce, the low-frequency range in the phonon spectrum of YCeH_x is slightly wider than that of LaCeH_x. The EPC constants of YCeH₈ at 100 GPa, YCeH₁₈ at 150 GPa, YCeH₂₀ at 300 GPa, LaCeH₈ at 100 GPa, and LaCeH₂₀ at

250 GPa are 0.41, 2.51, 1.02, 0.35, and 0.99, respectively. The EPC constant of YCeH_{18} is so significant compared to the other four phases. From the mode-resolved EPC constant λ_{qv} , we find that the largest contribution to the total EPC constant of YCeH_{18} comes from the optical phonon branch in the frequency range of 10 to 20 THz, which contributes about 0.64 (i.e., 25.7% to the total EPC constant). The rare-earth-atom associated vibrational modes with the frequencies of <10 THz for YCeH_{18} also have moderate contribution to the total EPC constant, as compared with the other four phases. In contrast, the contribution of rare-earth atoms to the EPC for YCeH_{20} with higher H content is only 0.09. When the pressure is increased from 150 GPa to 300 GPa, the phonons dominated by the H-atom-associated vibration in YCeH_{18} keep hardening, which can be seen from Fig. 4(a) and Fig. S11(c). The increase of pressure leads to a decrease of the EPC constant of YCeH_{18} , so that the EPC constant of YCeH_{18} at 300 GPa is very close to that of LaCeH_{20} at 300 GPa. The EPC constants of ACeH_8 ($A = \text{Y}$ and La) are so small, compared to ACeH_{18} and ACeH_{20} , since both the highest phonon frequencies and the H-derived electronic density of states in the former cases are lower than those in the latter cases. These results suggest that once the hydrogen atoms in metal hydrides simultaneously provide sufficient electron density of states at E_F and sufficient phonon density of states in the high-frequency region, a strong EPC strength would be achieved.

Based on the Allen-Dynes-modified McMillan formula [88] with a widely accepted value of the Coulomb pseudopotential μ^* ($\mu^* = 0.1$ used herein), the T_c values of $P4/mmm$ - YCeH_8 at 100 GPa, $P\bar{6}m2$ - YCeH_{18} at 150 GPa, $R\bar{3}m$ - YCeH_{20} at 300 GPa, $P4/mmm$ - LaCeH_8 at 100 GPa, and $P4/mmm$ - LaCeH_8 at 250 GPa are predicted to be 4.8, 173.8, 122.1, 1.8, and 116.1 K, respectively. We note that very recently three independent high-pressure experiments [68, 92, 93] on the La-Ce-H system have been reported, in which the measurement pressures by Chen *et al.* [68] and Bi *et al.* [92] were both less than 130 GPa and the observed T_c was around 180 K. One interesting thing is that even though these two research groups [68, 92] used different ratios of the starting materials for synthesis, the final measurement results were very close, suggesting that both of them synthesized probably the same high-temperature superconducting phase. Our calculation results show that at this pressure (130 GPa) the thermodynamically stable phase is LaCeH_{18} , which is not explored further here because the stabilization of this phase may involve anharmonic approximation effect not the focus of this work. The measurement pressure on La-Ce-H by Huang *et al.* [93] was in the range of 140-160 GPa. As mentioned above, LaCeH_{20} can be stabilized in this pressure range. A high-pressure experiment study [94] on the Y-Ce-H system has also been reported very recently, in which the observed T_c values are between 97-140 K. The predicted T_c value of YCeH_{18} by either the McM or AD formula shows a good agreement with this experiment data. To a certain extent, these experiment results show strong support to the validity of our theoretical prediction. In short, the high-pressure phases of LaCeH_{18} , LaCeH_{20} , and YCeH_{18} discovered computationally in this work have all been confirmed in the very recent high-

pressure experiments, among which LaCeH_{20} and YCeH_{18} are theoretically predicted for the first time.

C. Discussion

As presented above, ACeH_8 , YCeH_{18} and ACeH_{20} ($A = \text{La}$ and Y) have the space groups of $P4/mmm$, $P\bar{6}m2$ and $R\bar{3}m$, respectively, and the rare earth atoms are encased in the H_{18} , H_{29} and H_{32} cages, respectively. Herein we performed the COHP and integrated COHP (ICOHP) analyses to further investigate the chemical bonding in these cage structures. The critical bond lengths of some representative H-H, Ce-H, and A-H ($A = \text{La}, \text{Y}$) atom pairs and their corresponding ICOHP values that can reflect the bonding strength are shown in Figure 5. According to the convention of COHP analysis, the positive and negative values of $-\text{COHP}$ indicate the bonding and anti-bonding characteristics, respectively. As seen from Fig. 3, the H_{18} cage in YCeH_8 can be viewed as consisting of eight quadrangles and four hexagons. Accordingly, the H-H bond in the H_{18} cages can be roughly classified into three groups: i) H-H bonds shared by two neighboring quadrangles, ii) H-H bonds shared by two neighboring hexagons, and iii) H-H bonds shared by a quadrangle and a hexagon.

The H-H bond lengths in the first and second groups are denoted as D1 and D2, respectively, as indicated in Figs. S14(a) and S14(d) in the SM. These two distinct bond lengths D1 and D2 in YCeH_8 and LaCeH_8 at 100 GPa can be sorted in the following descending order: $D2(\text{LaCeH}_8) > D1(\text{YCeH}_8) \geq D1(\text{LaCeH}_8) > D2(\text{YCeH}_8)$. Although the H-H bonds with D1 in YCeH_8 and LaCeH_8 have the very close bond lengths, the projected COHPs for them shown in Figs. 5(a) and 5(c) indicate that this H-H bond in LaCeH_8 exhibits a stronger bonding interaction than in YCeH_8 because of the less anti-bonding states appearing just below E_F and a slightly greater absolute value of the corresponding ICOHP in LaCeH_8 . However, compared to the A-H and Ce-H bonds from their corresponding ICOHP values, the interaction of this H-H bond would be significantly weaker. For YCeH_{18} and ACeH_{20} with higher H content, the H-H bonds are significantly shrunken because of a higher pressure required to stabilize YCeH_{18} and ACeH_{20} , the ICOHP values of the H-H bonds in YCeH_{18} and ACeH_{20} are almost three times than those in ACeH_8 , and much less (and even no) anti-bonding states appear below E_F for the H-H bonds in YCeH_{20} (and LaCeH_{20}). From the H_{18} cages in ACeH_8 to the H_{29} cages in YCeH_{18} and H_{32} cages in ACeH_{20} , the cage size increases and the number of quadrangles (hexagons) decreases (increases) due to incorporating more H atoms. These results suggest that the H-H bonds within anti-bonding states in ACeH_8 could be much stabilized in YCeH_{18} and ACeH_{20} because they seem ready to be hybridized with the incorporated additional H atoms. In addition, YCeH_{20} has some remarkable anti-bonding states appearing around -11 eV for the Ce-H atom pair, as seen from Fig. 5(c), which mainly come from the hybridization between the H-1s and Ce-5p_x orbitals, suggesting that the semi-core states (such as 5p orbitals) of Ce in YCeH_{20} at the high pressure may contribute to the Ce-H bonding.

The crystal orbital bond index (COBI) can be used to quantify the strength of covalent bonds in covalently bonded solid materials. [74] The integrated-COBI (abbreviated to ICOBI) values for the H-H bonds in these caged structures of $ACeH_8$, $YCeH_{18}$ and $ACeH_{20}$ are less than 0.15, indicating very weak bonding interactions between H-H. The overall trend is that the ICOBI of H-H bonds increases with the increase of pressure, but the change is less than 0.02, suggesting that the effect of pressure on the H-H bonding is small. The similar trend is also observed from the analysis of ICOHP. One interesting thing is that the bonding strength of the H-H bonds in $R\bar{3}m$ - $YCeH_{20}$ in the pressure range of 300-400 GPa is slightly stronger than the one in $R\bar{3}m$ - $LaCeH_{20}$ according to both the electron localization function (ELF) and ICOHP analyses, although the corresponding ICOBI values in these two structures are quite close to each other and also exhibit a very weak dependence on the pressure.

The five superconducting compounds reported above, which are both thermodynamically and dynamically stable, are mainly of the $ACeH_8$, $ACeH_{18}$ and $ACeH_{20}$ types. The previously reported $ScCaH_8$ [52] and $YMgH_8$ [53] also have the same structure as $ACeH_8$. For the $ACeH_8$ type, there are three distinct types of H-H bonds, as mentioned above, in which the D1 decreases as the pressure increases, while the D2 exhibits a weaker dependence on the pressure. In addition, the bonding strength of the H-H bonds can also be described as the ELF.

Recently, Belli *et al.* [90] have proposed a strong correlation between the T_c value of superconducting hydride and the weak covalent H-H bonds. They also proposed a possible networking value ϕ , which is defined as the highest value of the ELF that creates an isosurface spanning through the whole crystal in all three Cartesian directions, to describe the nature of the H-H bond in hydrides. As noted by Belli *et al.*, [90] the precise acquisition of the ϕ value is not uniquely defined. From the radial distribution function of H atoms in our studied $YCeH_x$ and $LaCeH_x$ phases as a function of pressure, as presented in Fig. S14 in the SM, we note that within the radial range of 3 Å there is a main peak representing the most important distribution of H-H bond lengths. In this way, we obtain the ϕ value by taking the average of all ELF values at the valley points of the lines plots of ELF along different H-H bonds that correspond to such a main peak. And according to the model proposed by Belli *et al.*, [90] the T_c of metal hydride can be predicted by the following equation with an accuracy in the range of 60 K:

$$T_c = 750\phi H_f \sqrt[1/3]{H_{DOS}} - 85, \quad (9)$$

where H_f is the hydrogen fraction and H_{DOS} is the hydrogen fraction of the total DOS at E_F . As presented in Table I, the network values ϕ of our studied phases are all less than 0.5 and they are very close. Consequently, the T_c values predicted by Eq. (9) are more significantly affected by the contribution of H_{DOS} . We also noted that the T_c values predicted by Eq. (9) are still somewhat deviation from those predicted by the AD formula, i.e., Eq. (3). Through the examination on $YCeH_{18}$ at 150 and 300 GPa, it can be seen that when the pressure

increases, the H-H distance decreases, the overall network ϕ value exhibits an increasing trend, and the contribution of H to the density of states at E_F also increases. And thus the Eq. (9) based on ELF predicts that the T_c for $YCeH_{18}$ increases with the increase of pressure, which is opposite to the trend in the prediction of the AD formula. This indicates that one possible limitation in the use of Eq. (9) to predict T_c may be the pressure-dependence of T_c . From the predicted results of Peng *et al.* [26] for all binary rare-earth metal hydrides, a trend can be seen that the elements containing more f electrons exhibit a suppressing effect on the T_c value. However, the dataset to build Eq. (9) in the work of Belli *et al.* [90] contains too few the f-electron-containing cases (i.e., only CeH_9 and PrH_9 included therein). Therefore, the T_c does exhibit a certain relationship with the ϕ and H_{DOS} values, however, the generalization of Eq. (9) to the pressure-dependence and the f-electron-containing systems needs a further improvement.

IV. CONCLUSION

In summary, we employed the evolutionary algorithm and first-principles calculations to study the ternary phase diagrams of $YCeH_x$ and $LaCeH_x$ systems under the pressure range of 100-400 GPa. The clathrate structure surrounded by H_{18} , H_{29} , and H_{32} can maintain thermodynamic stability in the searched pressure range. These cage structures correspond to $YCeH_8$, $YCeH_{18}$, $YCeH_{20}$, $LaCeH_8$, $LaCeH_{18}$, $LaCeH_{20}$, respectively. However, under the harmonic approximation, $LaCeH_{18}$ cannot achieve dynamic stability. We further studied the superconductivity of $YCeH_8$, $YCeH_{18}$, $YCeH_{20}$, $LaCeH_8$, and $LaCeH_{20}$. The results show that all four can achieve high temperature superconductivity, and $P\bar{6}m2$ - $YCeH_{18}$ can have the highest 173 K at 150GPa. In addition, in terms of the structure of these phases, $P4/mmm$ - $YCeH_8$, $P4/mmm$ - $LaCeH_8$, $P\bar{6}m2$ - $YCeH_{18}$, $P4/mmm$ - $YCeH_{20}$ can all be obtained by element replacement in binary superconducting hydrides. In other words, the search for new superconducting hydrides can start from the combination of binary superconducting hydrides. When two kinds of binary superconducting hydrides with similar properties are combined together, it is possible to form a novel stable three ternary hydride.

ACKNOWLEDGMENTS

The computations in this work have been performed using the facilities of Research Center for Advanced Computing Infrastructure (RCACI) at JAIST. P.S. is grateful for financial support from Grant-in-Aid for JSPS Research Fellow (JSPS KAKENHI Grant No. 22J10527). K.H. is grateful for financial support from the HPCI System Research Project (Project ID: hp190169) and MEXT-KAKENHI (JP16H06439, JP17K17762, JP19K05029, and JP19H05169). R.M. is grateful for financial supports from MEXT-KAKENHI (19H04692 and 16KK0097), FLAG-SHIP2020 (project nos. hp1 90169 and hp190167 at K-computer), Toyota Motor Corporation, I-O DATA Founda-

tion, the Air Force Office of Scientific Research (AFOSR-

AOARD/FA2386-17-1-4049;FA2386-19-1-4015), and JSPS Bilateral Joint Projects (with India DST).

-
- [1] M. Tinkham, *Introduction to superconductivity* (Courier Corporation, 2004).
- [2] P. G. D. Gennes, *Superconductivity of Metals and Alloys* (CRC Press, 2018).
- [3] J. Linder and J. W. A. Robinson, *Nat. Phys.* **11**, 307 (2015).
- [4] B. Josephson, *Phys. Lett* **1**, 251 (1962).
- [5] A. Bergen, R. Andersen, M. Bauer, H. Boy, M. ter Brake, P. Brutsaert, C. Bühner, M. Dhallé, J. Hansen, H. ten Kate, J. Kellers, J. Krause, E. Krooshoop, C. Kruse, H. Kylling, M. Pilas, H. Pütz, A. Rebsdorf, M. Reckhard, E. Seitz, H. Springer, X. Song, N. Tzabar, S. Wessel, J. Wiezoreck, T. Winkler, and K. Yagotyntsev, *Supercond. Sci. Technol.* **32**, 125006 (2019).
- [6] M. R. Islam, Y. Guo, and J. Zhu, *Renew. Sust. Energ. Rev.* **33**, 161 (2014).
- [7] H. Thomas, A. Marian, A. Chervyakov, S. Stückrad, D. Salmieri, and C. Rubbia, *Renew. Sust. Energ. Rev.* **55**, 59 (2016).
- [8] M. Tinkham, *Phys. Rev. Lett.* **61**, 1658 (1988).
- [9] S. S. Kalsi, *Applications of high temperature superconductors to electric power equipment* (John Wiley & Sons, 2011).
- [10] J. A. Flores-Livas, L. Boeri, A. Sanna, G. Profeta, R. Arita, and M. Eremets, *Phys. Rep.* **856**, 1 (2020).
- [11] J. Bardeen, *Phys. Rev.* **97**, 1724 (1955).
- [12] L. N. Cooper, *Phys. Rev.* **104**, 1189 (1956).
- [13] J. Bardeen, L. N. Cooper, and J. R. Schrieffer, *Phys. Rev.* **106**, 162 (1957).
- [14] J. Bardeen, L. N. Cooper, and J. R. Schrieffer, *Phys. Rev.* **108**, 1175 (1957).
- [15] N. W. Ashcroft, *Phys. Rev. Lett.* **21**, 1748 (1968).
- [16] E. Wigner and H. B. Huntington, *J. Chem. Phys.* **3**, 764 (1935).
- [17] P. Loubeyre, R. LeToullec, D. Hausermann, M. Hanfland, R. J. Hemley, H. K. Mao, and L. W. Finger, *Nature* **383**, 702 (1996).
- [18] J. McMinis, R. C. Clay, D. Lee, and M. A. Morales, *Phys. Rev. Lett.* **114**, 105305 (2015).
- [19] M. I. Eremets and I. A. Troyan, *Nat. Mater.* **10**, 927 (2011).
- [20] P. Dalladay-Simpson, R. T. Howie, and E. Gregoryanz, *Nature* **529**, 63 (2016).
- [21] R. P. Dias and I. F. Silvera, *Science* **355**, 715 (2017).
- [22] D. Castelvetti, *Nature* **542**, 17 (2017).
- [23] P. M. Celliers, M. Millot, S. Brygoo, R. S. McWilliams, D. E. Fratanduono, J. R. Rygg, A. F. Goncharov, P. Loubeyre, J. H. Eggert, J. L. Peterson, N. B. Meezan, S. L. Pape, G. W. Collins, R. Jeanloz, and R. J. Hemley, *Science* **361**, 677 (2018).
- [24] N. W. Ashcroft, *Phys. Rev. Lett.* **92**, 187002 (2004).
- [25] D. V. Semenov, I. A. Kruglov, I. A. Savkin, A. G. Kvashnin, and A. R. Oganov, *Curr. Opin. Solid State Mater. Sci.* **24**, 100808 (2020).
- [26] F. Peng, Y. Sun, C. J. Pickard, R. J. Needs, Q. Wu, and Y. Ma, *Phys. Rev. Lett.* **119**, 107001 (2017).
- [27] J. Zhang, J. M. McMahon, A. R. Oganov, X. Li, X. Dong, H. Dong, and S. Wang, *Phys. Rev. B* **101**, 134108 (2020).
- [28] X. Li and F. Peng, *Inorg. Chem.* **56**, 13759 (2017).
- [29] S. Yu, X. Jia, G. Frapper, D. Li, A. R. Oganov, Q. Zeng, and L. Zhang, *Sci. Rep.* **5**, 1 (2015).
- [30] M. Einaga, M. Sakata, T. Ishikawa, K. Shimizu, M. I. Eremets, A. P. Drozdov, I. A. Troyan, N. Hirao, and Y. Ohishi, *Nat. Phys.* **12**, 835 (2016).
- [31] A. P. Drozdov, M. I. Eremets, I. A. Troyan, V. Ksenofontov, and S. I. Shylin, *Nature* **525**, 73 (2015).
- [32] A. P. Drozdov, P. P. Kong, V. S. Minkov, S. P. Besedin, M. A. Kuzovnikov, S. Mozaffari, L. Balicas, F. F. Balakirev, D. E. Graf, V. B. Prakapenka, E. Greenberg, D. A. Knyazev, M. Tkacz, and M. I. Eremets, *Nature* **569**, 528 (2019).
- [33] N. P. Salke, M. M. D. Esfahani, Y. Zhang, I. A. Kruglov, J. Zhou, Y. Wang, E. Greenberg, V. B. Prakapenka, J. Liu, A. R. Oganov, and J.-F. Lin, *Nat. Commun.* **10**, 1 (2019).
- [34] W. Chen, D. V. Semenov, A. G. Kvashnin, X. Huang, I. A. Kruglov, M. Galasso, H. Song, D. Duan, A. F. Goncharov, V. B. Prakapenka, A. R. Oganov, and T. Cui, *Nat. Commun.* **12**, 1 (2021).
- [35] M. Shao, W. Chen, K. Zhang, X. Huang, and T. Cui, *Phys. Rev. B* **104**, 174509 (2021).
- [36] M. Shao, S. Chen, W. Chen, K. Zhang, X. Huang, and T. Cui, *Inorg. Chem.* **60**, 15330 (2021).
- [37] I. A. Troyan, D. V. Semenov, A. G. Kvashnin, A. V. Sadakov, O. A. Sobolevskiy, V. M. Pudalov, A. G. Ivanova, V. B. Prakapenka, E. Greenberg, A. G. Gavriluk, I. S. Lyubutin, V. V. Struzhkin, A. Bergara, I. Errea, R. Bianco, M. Calandra, F. Mauri, L. Monacelli, R. Akashi, and A. R. Oganov, *Adv. Mater.* **33**, 2006832 (2021).
- [38] W. Chen, D. Semenov, X. Huang, H. Shu, X. Li, D. Duan, T. Cui, and A. Oganov, *Phys. Rev. Lett.* **127**, 117001 (2021).
- [39] P. Kong, V. S. Minkov, M. A. Kuzovnikov, A. P. Drozdov, S. P. Besedin, S. Mozaffari, L. Balicas, F. F. Balakirev, V. B. Prakapenka, S. Chariton, D. A. Knyazev, E. Greenberg, and M. I. Eremets, *Nat. Commun.* **12**, 1 (2021).
- [40] Y. Li, J. Hao, H. Liu, Y. Li, and Y. Ma, *J. Chem. Phys.* **140**, 174712 (2014).
- [41] M. Somayazulu, M. Ahart, A. K. Mishra, Z. M. Geballe, M. Baldini, Y. Meng, V. V. Struzhkin, and R. J. Hemley, *Phys. Rev. Lett.* **122**, 027001 (2019).
- [42] P. Song, Z. Hou, P. B. de Castro, K. Nakano, K. Hongo, Y. Takano, and R. Maezono, *Chem. Mater.* **33**, 9501 (2021).
- [43] Y. Ma, D. Duan, Z. Shao, D. Li, L. Wang, H. Yu, F. Tian, H. Xie, B. Liu, and T. Cui, *Phys. Chem. Chem. Phys.* **19**, 27406 (2017).
- [44] Y. Ma, D. Duan, Z. Shao, H. Yu, H. Liu, F. Tian, X. Huang, D. Li, B. Liu, and T. Cui, *Phys. Rev. B* **96**, 144518 (2017).
- [45] Z. Shao, D. Duan, Y. Ma, H. Yu, H. Song, H. Xie, D. Li, F. Tian, B. Liu, and T. Cui, *npj Comput. Mater.* **5**, 1 (2019).
- [46] J. Zheng, W. Sun, X. Dou, A.-J. Mao, and C. Lu, *J. Phys. Chem. C* **125**, 3150 (2021).
- [47] M. Rahm, R. Hoffmann, and N. W. Ashcroft, *J. Am. Chem. Soc.* **139**, 8740 (2017).
- [48] X. Liang, A. Bergara, X. Wei, X. Song, L. Wang, R. Sun, H. Liu, R. J. Hemley, L. Wang, G. Gao, and Y. Tian, *Phys. Rev. B* **104**, 134501 (2021).
- [49] Y. Sun, J. Lv, Y. Xie, H. Liu, and Y. Ma, *Phys. Rev. Lett.* **123**, 097001 (2019).
- [50] X. Liang, S. Zhao, C. Shao, A. Bergara, H. Liu, L. Wang, R. Sun, Y. Zhang, Y. Gao, Z. Zhao, X.-F. Zhou, J. He, D. Yu, G. Gao, and Y. Tian, *Phys. Rev. B* **100**, 184502 (2019).
- [51] Y. K. Wei, L. Q. Jia, Y. Y. Fang, L. J. Wang, Z. X. Qian, J. N. Yuan, G. Selvaraj, G. F. Ji, and D. Q. Wei, *Int. J. Quantum*

- Chem.* **121**, 26459 (2020).
- [52] L.-T. Shi, Y.-K. Wei, A.-K. Liang, R. Turnbull, C. Cheng, X.-R. Chen, and G.-F. Ji, *J. Mater. Chem. C* **9**, 7284 (2021).
- [53] P. Song, Z. Hou, P. B. de Castro, K. Nakano, Y. Takano, R. Maezono, and K. Hongo, *Adv. Theory Simul.* **5**, 2100364 (2022).
- [54] D. V. Semenok, I. A. Troyan, A. G. Ivanova, A. G. Kvashnin, I. A. Kruglov, M. Hanfland, A. V. Sadakov, O. A. Sobolevskiy, K. S. Pervakov, I. S. Lyubutin, K. V. Glazyrin, N. Giordano, D. N. Karimov, A. L. Vasiliev, R. Akashi, V. M. Pudalov, and A. R. Oganov, *Mater. Today* **48**, 18 (2021).
- [55] X. Liang, A. Bergara, L. Wang, B. Wen, Z. Zhao, X.-F. Zhou, J. He, G. Gao, and Y. Tian, *Phys. Rev. B* **99**, 100505 (2019).
- [56] M.-J. Jiang, H.-L. Tian, Y.-L. Hai, N. Lu, P.-F. Tong, S.-Y. Wu, W.-J. Li, C.-L. Yang, and G.-H. Zhong, *ACS Appl. Electron. Mater.* **3**, 4172 (2021).
- [57] W. Cui, T. Bi, J. Shi, Y. Li, H. Liu, E. Zurek, and R. J. Hemley, *Phys. Rev. B* **101**, 134504 (2020).
- [58] S. D. Cataldo, W. von der Linden, and L. Boeri, *Phys. Rev. B* **102**, 014516 (2020).
- [59] P. Song, Z. Hou, P. B. de Castro, K. Nakano, K. Hongo, Y. Takano, and R. Maezono, *J. Phys. Chem. C* **126**, 2747 (2022).
- [60] S. D. Cataldo, W. von der Linden, and L. Boeri, *Npj Comput. Mater.* **8**, 1 (2022).
- [61] R. Vocaturato, C. Tresca, G. Ghiringhelli, and G. Profeta, *J. Appl. Phys.* **131**, 033903 (2022).
- [62] E. Snider, N. Dasenbrock-Gammon, R. McBride, M. Debessai, H. Vindana, K. Vencatasamy, K. V. Lawler, A. Salamat, and R. P. Dias, *Nature* **586**, 373 (2020).
- [63] J. E. Hirsch and F. Marsiglio, *Nature* **596**, E9 (2021).
- [64] J. E. Hirsch, *Europhys. Lett.* **137**, 36001 (2022).
- [65] A. Nakanishi, T. Ishikawa, and K. Shimizu, *J. Phys. Soc. Jpn.* **87**, 124711 (2018).
- [66] M. Amsler, *Phys. Rev. B* **99**, 060102 (2019).
- [67] H. Guan, Y. Sun, and H. Liu, *Phys. Rev. Res.* **3**, 043102 (2021).
- [68] W. Chen, X. Huang, D. V. Semenok, S. Chen, K. Zhang, A. R. Oganov, and T. Cui, arXiv preprint arXiv:2203.14353 (2022).
- [69] C. W. Glass, A. R. Oganov, and N. Hansen, *Comput. Phys. Commun.* **175**, 713 (2006).
- [70] A. O. Lyakhov, A. R. Oganov, H. T. Stokes, and Q. Zhu, *Comput. Phys. Commun.* **184**, 1172 (2013).
- [71] J. P. Perdew, K. Burke, and M. Ernzerhof, *Phys. Rev. Lett.* **77**, 3865 (1996).
- [72] G. Kresse and J. Furthmüller, *Phys. Rev. B* **54**, 11169 (1996).
- [73] G. Kresse and D. Joubert, *Phys. Rev. B* **59**, 1758 (1999).
- [74] P. C. Müller, C. Ertural, J. Hempelmann, and R. Dronskowski, *J. Phys. Chem. C* **125**, 7959 (2021).
- [75] S. L. Dudarev, G. A. Botton, S. Y. Savrasov, C. J. Humphreys, and A. P. Sutton, *Phys. Rev. B* **57**, 1505 (1998).
- [76] I. Timrov, N. Marzari, and M. Cococcioni, arXiv preprint arXiv:2203.15684 (2022).
- [77] C. Wang, S. Liu, H. Jeon, S. Yi, Y. Bang, and J.-H. Cho, *Phys. Rev. B* **104**, 1020504 (2021).
- [78] Y. Chen, Q.-M. Hu, and R. Yang, *Phys. Rev. Lett.* **109**, 157004 (2012).
- [79] Y. K. Vohra, S. L. Beaver, J. Akella, C. A. Ruddle, and S. T. Weir, *J. Appl. Phys.* **85**, 2451 (1999).
- [80] L. Chen, T. Liang, Z. Zhang, H. Song, Z. Liu, Q. Jiang, Y. Chen, and D. Duan, *J. Phys.: Condens. Matter* **34**, 204005 (2022).
- [81] C. J. Pickard and R. J. Needs, *Nat. Phys.* **3**, 473 (2007).
- [82] A. R. Akbarzadeh, V. Ozoliņš, and C. Wolverton, *Adv. Mater.* **19**, 3233 (2007).
- [83] P. Virtanen, R. Gommers, T. E. Oliphant, M. Haberland, T. Reddy, D. Cournapeau, E. Burovski, P. Peterson, W. Weckesser, J. Bright, S. J. van der Walt, M. Brett, J. Wilson, K. J. Millman, N. Mayorov, A. R. J. Nelson, E. Jones, R. Kern, E. Larson, C. J. Carey, Í. Polat, Y. Feng, E. W. Moore, J. VanderPlas, D. Laxalde, J. Perktold, R. Cimrman, I. Henriksen, E. A. Quintero, C. R. Harris, A. M. Archibald, A. H. Ribeiro, F. Pedregosa, and P. van Mulbregt, *Nat. Methods* **17**, 352 (2020).
- [84] A. Togo and I. Tanaka, *Scr. Mater.* **108**, 1 (2015).
- [85] P. Giannozzi, S. Baroni, N. Bonini, M. Calandra, R. Car, C. Cavazzoni, D. Ceresoli, G. L. Chiarotti, M. Cococcioni, I. Dabo, A. D. Corso, S. de Gironcoli, S. Fabris, G. Fratesi, R. Gebauer, U. Gerstmann, C. Gougousis, A. Kokalj, M. Lazzeri, L. Martin-Samos, N. Marzari, F. Mauri, R. Mazzarello, S. Paolini, A. Pasquarello, L. Paulatto, C. Sbraccia, S. Scandolo, G. Sclauzero, A. P. Seitsonen, A. Smogunov, P. Umari, and R. M. Wentzcovitch, *J. Phys.: Condens. Matter* **21**, 395502 (2009).
- [86] A. D. Corso, *Comp. Mater. Sci.* **95**, 337 (2014).
- [87] W. L. McMillan, *Phys. Rev.* **167**, 331 (1968).
- [88] P. B. Allen and R. C. Dynes, *Phys. Rev. B* **12**, 905 (1975).
- [89] H. Liu, I. I. Naumov, R. Hoffmann, N. W. Ashcroft, and R. J. Hemley, *Proc. Natl. Acad. Sci.* **114**, 6990 (2017).
- [90] F. Belli, T. Novoa, J. Contreras-García, and I. Errea, *Nat. Commun.* **12**, 5381 (2021).
- [91] B. Li, Z. Miao, L. Ti, S. Liu, J. Chen, Z. Shi, and E. Gregoryanz, *J. Appl. Phys.* **126**, 235901 (2019).
- [92] J. Bi, Y. Nakamoto, K. Shimizu, M. Zhou, H. Wang, G. Liu, and Y. Ma, arXiv preprint arXiv:2204.04623 (2022).
- [93] G. Huang, T. Luo, P. Dalladay Simpson, L. Chen, Z. Cao, D. Peng, F. A. Gorelli, G. Zhong, H. Lin, and X. Chen, arXiv preprint arXiv:2208.05199 (2022).
- [94] L. Chen, T. Luo, P. Dalladay Simpson, G. Huang, Z. Cao, D. Peng, F. A. Gorelli, G. Zhong, H. Lin, and X. Chen, arXiv preprint arXiv:2208.05191 (2022).

TABLE I. Superconducting transition temperature (T_c) predicted by the original McMillan formula (abbreviated to McM), [87] the Allen-Dynes-modified McMillan (McM) formula (abbreviated to AD), [88] and the model (i.e., Eq. (9)) proposed by Belli *et al.*, [90] (abbreviated to ELF) for A -Ce-H ($A = Y$ and La) at some selected pressures. Accordingly, the values of some key parameters contained in these formulas and model are also listed.

Phase	Space group	P (GPa)	N_{atom}	d_{H-H} Å	ϕ	H_{DOS}	λ	ω_{log} (K)	T_c (ELF) (K)	T_c (McM) (K)	T_c (AD) (K)
YCeH ₈	$P4/mmm$	100	20	1.52	0.40	9.5%	0.41	987.5	24.5	4.7	4.8
YCeH ₁₈	$P\bar{6}m2$	150	22	1.07	0.43	34.4%	2.51	812.2	118.3	133.8	173.8
YCeH ₁₈	$P\bar{6}m2$	300	22	1.05	0.46	39.2%	0.97	1547.7	142.2	103	110
YCeH ₂₀	$R\bar{3}m$	300	66	1.05	0.45	38.2%	1.03	1595.2	137.6	114.2	122.1
LaCeH ₈	$P4/mmm$	100	20	1.56	0.38	11.2%	0.35	975.8	24.9	1.73	1.76
LaCeH ₂₀	$R\bar{3}m$	250	66	1.06	0.48	34.7%	1.00	1566.9	145.0	109.1	116.1

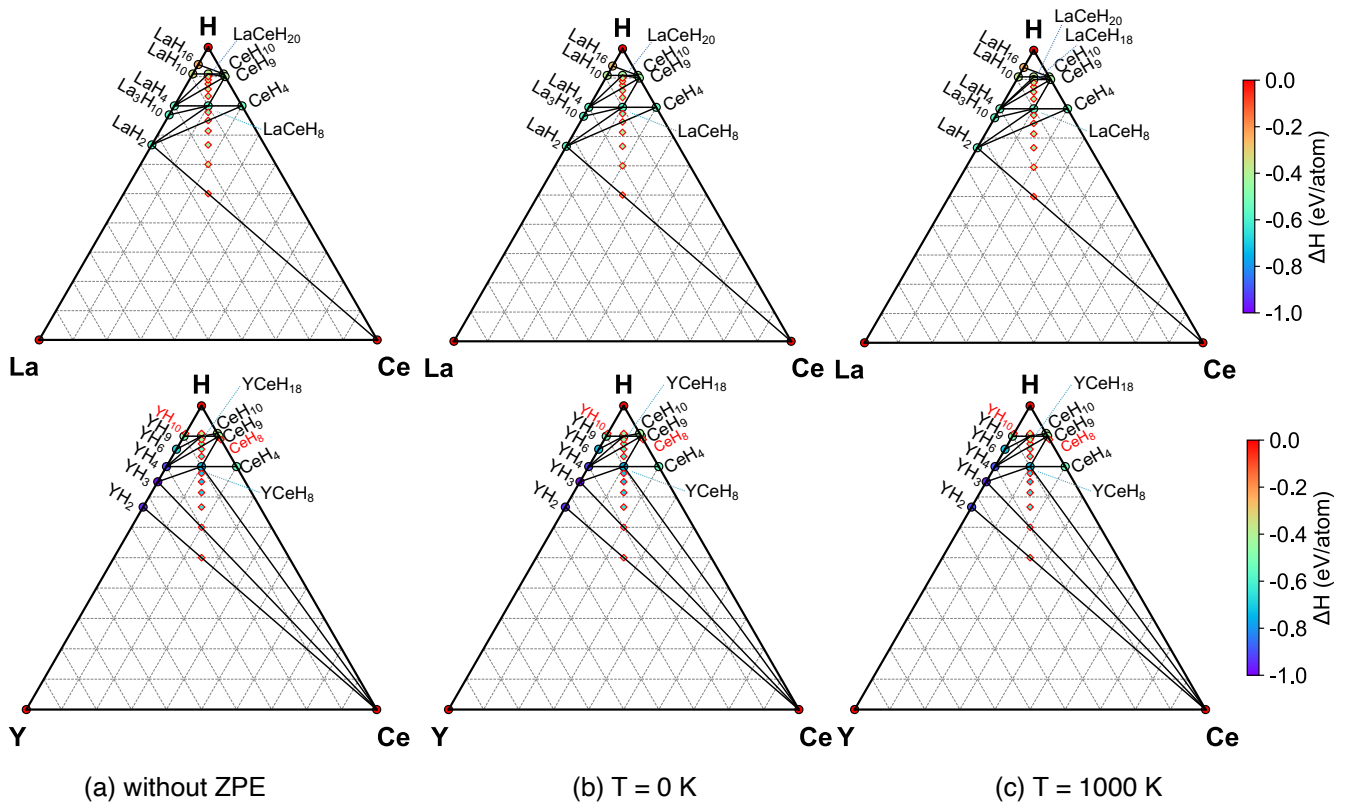


FIG. 1. Ternary convex hulls of YCeH_x and LaCeH_x at 200 GPa. The stable and metastable phases are highlighted by the symbols of circles and red diamond, respectively. The right panels are the convex hull at 0 K (with the correction of zero-point energy) and 1000 K.

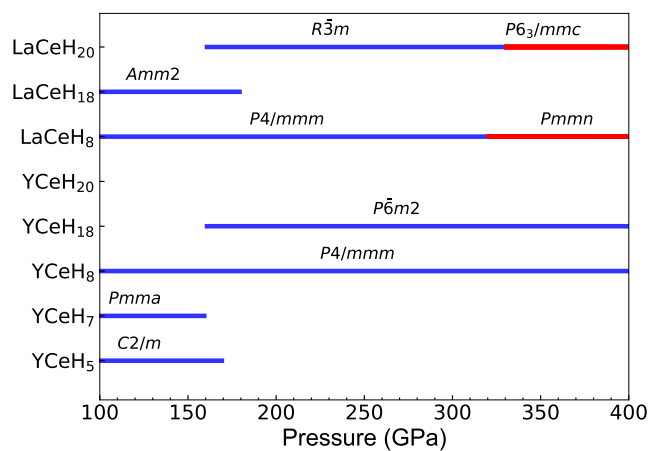


FIG. 2. Phase diagram of YCeH_x and LaCeH_x in the pressure range from 100 to 400 GPa.

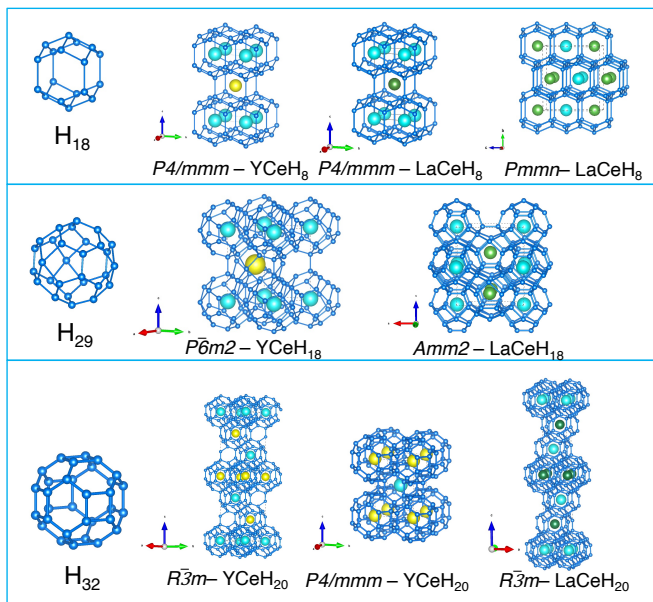


FIG. 3. The clathrate structures of stable YCeH_x and LaCeH_x .

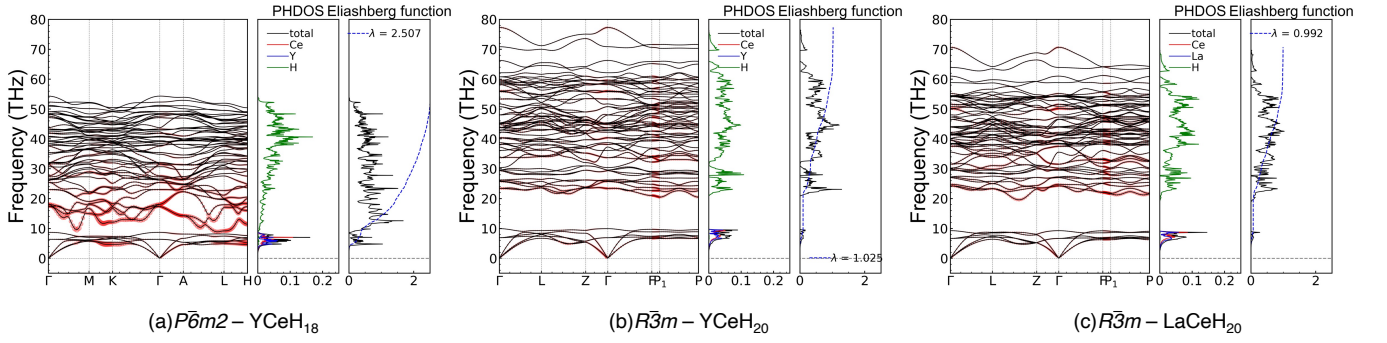


FIG. 4. The phonon spectra with a projection of mode-resolved EPC constant λ_{qv} (red circle), atom-projected phonon density of states (PHDOS), and Eliashberg function of (a) $P\bar{6}m2$ - YCeH_{18} at 150 GPa, (b) $R\bar{3}m$ - YCeH_{20} at 300 GPa, and (c) $R\bar{3}m$ - LaCeH_{20} at 250 GPa. The mode-resolved EPC constant λ_{qv} is defined as $\lambda_{qv} = \frac{\gamma_{qv}}{\pi \hbar N(E_F) \omega_{qv}^2}$, where γ_{qv} is phonon linewidth, $N(E_F)$ is the DOS at the Fermi level, and ω_{qv} is the mode-resolve phonon frequency.

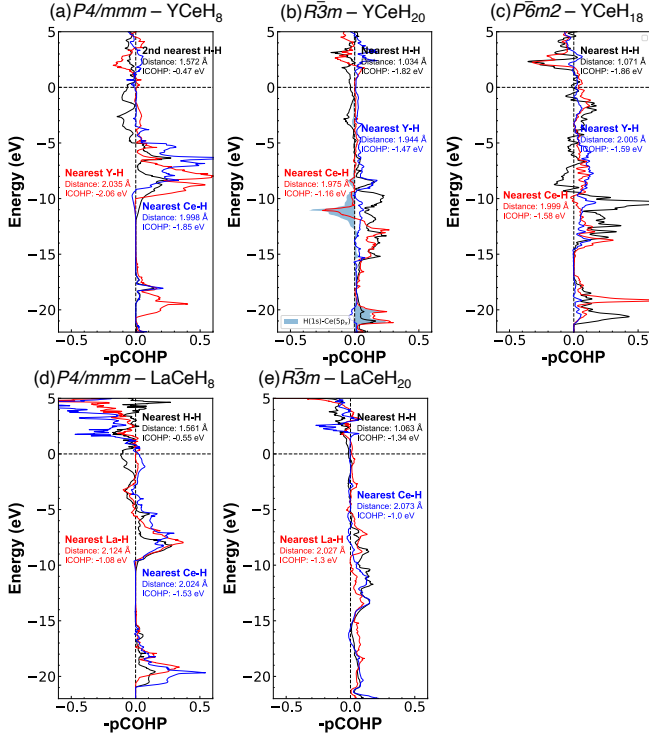


FIG. 5. The Crystal Orbital Hamilton Population (COHP) of some representative atom pairs (H-H, Y-H, La-H, and Ce-H) in $P4/mmm$ - YCeH_8 , $P\bar{6}m2$ - YCeH_{18} , $R\bar{3}m$ - YCeH_{20} , $P4/mmm$ - LaCeH_8 , and $R\bar{3}m$ - LaCeH_{20} at the pressure of 100, 150, 300, 100, and 250 GPa, respectively.